A. Supplementary Material

Objective term definitions and weights

The objective function consisted of three weighted terms. The effort term J_{effort} minimized muscular effort, estimated as squared muscle activation (van den Bogert, 2025; Dorschky et al., 2019), weighted by relative muscle volume (Nitschke et al., 2020), and normalized by the squared nominal treadmill speed v_{nom} (Dorschky et al., 2019):

$$J_{\mathrm{effort}} = \frac{1}{v_{\mathrm{nom}}^2} \int_0^{T_{\mathrm{sim}}} \sum_{i=1}^{N_{\mathrm{muscles}}} \left(\frac{F_{\mathrm{ISO},i} l_{\mathrm{CE,opt},i}}{\sum_{i=1}^{N_{\mathrm{muscles}}} F_{\mathrm{ISO},i} l_{\mathrm{CE,opt},i}} a_i(t)^2 \right) dt, \tag{1}$$

where $a_i(t)$ denotes the activation of muscle i, $F_{\mathrm{ISO},i}$ its maximum isometric force, and $l_{\mathrm{CE,opt},i}$ its optimal contractile element length. Relative muscle volume was estimated from $F_{\mathrm{ISO},i} l_{\mathrm{CE,opt},i}$ (Nitschke et al., 2020). N_{muscles} denotes the number of muscles and T_{sim} the simulated stride duration.

Both tracking terms, J_{angles} and J_{GRF}, minimized the differences between the simulated trajectories and the corresponding mean experimental trajectories. Similar to previous work, the tracking error was normalized by the experimental standard deviation:

$$J_{\mathrm{track}} = \frac{1}{T_{\mathrm{sim}}} \int_0^{T_{\mathrm{sim}}} \sum_{i=1}^{N_{\mathrm{track}}} \left(\frac{y_{\mathrm{sim},i}(t) - \mu_{y_{\mathrm{meas},i}}(t)}{\sigma_{y_{\mathrm{meas},i}}(t)} \right)^2 dt, \tag{2}$$

where $y_{\mathrm{sim},i}(t)$ denotes the simulated trajectory of tracked variable i, and $\mu_{y_{\mathrm{meas},i}}(t)$ and $\sigma_{y_{\mathrm{meas},i}}(t)$ denote the corresponding experimental mean and standard deviation, respectively. N_{track} denotes the number of variables included in the respective tracking term.

For joint-angle tracking, the experimental means and standard deviations were taken from the representative gait data reported by Winter (1987). For GRF tracking, participant-specific experimental trajectories were used. For the GRF signals, the standard deviation was set to 1 to ensure close tracking of the measured mean throughout the gait cycle. To reduce differences in scale between participants, GRFs were additionally normalized to body weight before computing J_{GRF}.

The weights of the individual objective terms are reported in Table 1.

The magnitude of the weighting factors does not directly indicate the contribution of each term to the final objective, due to differences in the units and magnitudes of the tracked signals. Despite the comparatively large weighting factor for GRF tracking, effort was the main contributor, accounting for more than 60% of the total objective.

Table 1
Weighting factors for the individual objective terms for each simulation.

	w_{effort}	w_{GRF}	w_{angle}
low-stiffness simulation (contact stiffness parameter 5×10^5)	300	1×10^3	0.5
ideal treadmill simulation (contact stiffness parameter 2×10^6)	300	5×10^3	0.5
realistic treadmill simulation (contact stiffness parameter 2×10^6)	300	5×10^3	0.5

AP GRF interpolation for the treadmill controller in simulations

In our simulations, the anterior-posterior (AP) ground reaction forces (GRFs) often showed a sharp spike during the loading response (Figure 1a), which is likely an artifact of the ground contact model rather than a meaningful signal and is not observed in experimental human GRFs. Such a spike has also been reported in other gait simulations (e.g., (Dorn et al., 2015; Ackermann and van den Bogert, 2010; Miller, 2014; Geyer and Herr, 2010)).

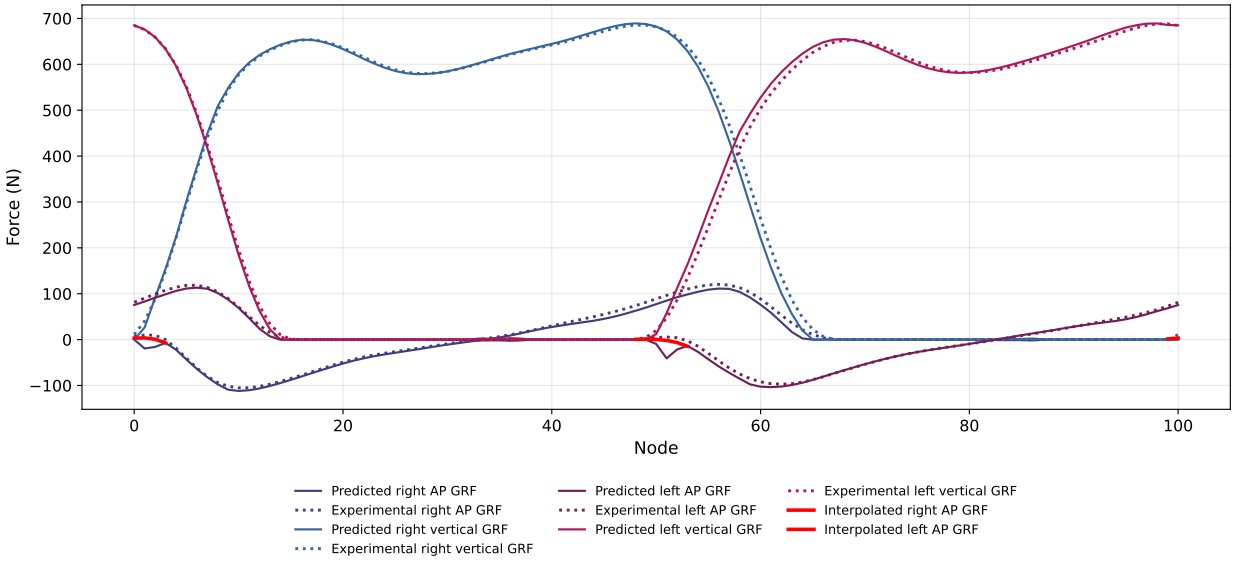
However, since the treadmill controller uses the rate of change of the AP and vertical GRFs, it is sensitive to rapid changes in these signals, and such a spike would produce an unrealistic and exaggerated belt-speed response. We therefore interpolated these regions before passing the GRF signal into the realistic treadmill controller.

To identify the post-heel-strike AP-GRF region requiring interpolation, foot contact was first detected when the vertical GRF exceeded 10 N. The sample immediately preceding foot contact was used as the start of the interpolation region.

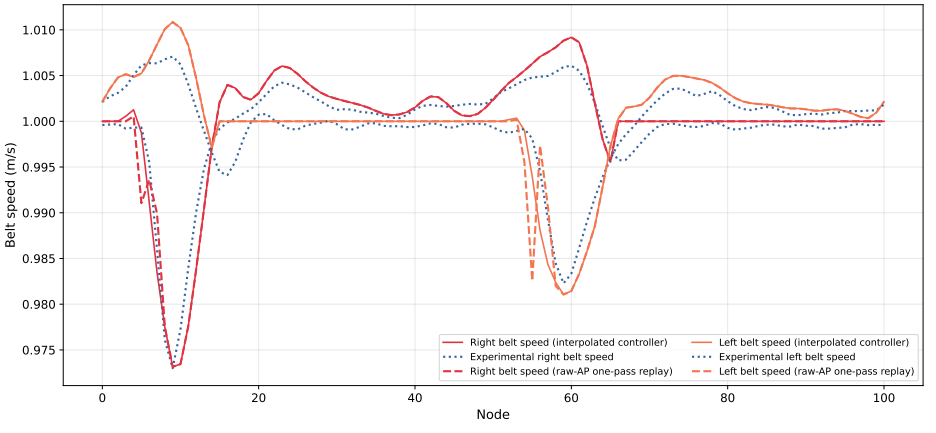
Starting from heel strike, local maxima in the AP GRF were identified as potential endpoints of the interpolation region by a change in the sign of the discrete derivative from positive to negative. When multiple maxima were present, the maximum with the largest positive-to-negative change in the derivative was selected as the end of the interpolation region.

The AP-GRF samples between these start and end points were replaced using cubic-spline interpolation based on the five preceding and six subsequent unaffected samples (Figure 1a). All indices were treated periodically across the gait-cycle boundary.

Figure 1b shows a comparison of the predicted belt-speed variation with and without interpolation of the GRF signal.



(a) Experimental and simulated ground reaction forces for the right and left legs. The region of the anterior-posterior ground reaction force interpolated before being passed to the treadmill controller is shown in red.



(b) Experimental and predicted belt speeds. Interpolating the sharp AP-GRF spike during the loading response resulted in realistic belt-speed variations, whereas using the original GRF signal produced an additional sharp change in belt speed.

Figure 1: Example of experimental and simulated ground reaction forces and belt speeds for one participant walking at 1 m/s.

Excluded simulation trials

The solver did not find a solution for participant 10 at 1.0 and 1.4-1.8 m/s. Toe-walking occurred with the realistic treadmill for participant 5 at 1.2 m/s, participant 7 at 1.4 m/s, and participant 8 at 1.6 m/s. As written in the main text, we excluded both the realistic and ideal trial in those cases.

References

Ackermann, M. and van den Bogert, A. J. (2010). Optimality principles for model-based prediction of human gait. *Journal of Biomechanics*, 43(6):1055–1060.

Dorn, T. W., Wang, J. M., Hicks, J. L., and Delp, S. L. (2015). Predictive simulation generates human adaptations during loaded and inclined walking. *PloS one*, 10(4):e0121407.

Dorschky, E., Nitschke, M., Seifer, A.-K., van den Bogert, A. J., and Eskofier, B. M. (2019). Estimation of gait kinematics and kinetics from inertial sensor data using optimal control of musculoskeletal models. *Journal of Biomechanics*, 95:109278.

Geyer, H. and Herr, H. (2010). A muscle-reflex model that encodes principles of legged mechanics produces human walking dynamics and muscle activities. *IEEE Transactions on Neural Systems and Rehabilitation Engineering*, 18(3):263–273.

Miller, R. H. (2014). A comparison of muscle energy models for simulating human walking in three dimensions. *Journal of Biomechanics*, 47(6):1373–1381.

Nitschke, M., Dorschky, E., Heinrich, D., Schlarb, H., Eskofier, B. M., Koelewijn, A. D., and Van den Bogert, A. J. (2020). Efficient trajectory optimization for curved running using a 3d musculoskeletal model with implicit dynamics. *Scientific reports*, 10(1):17655.

van den Bogert, A. J. (2025). Strange effects of activation dynamics on musculoskeletal trajectory optimization. *bioRxiv*.

Winter, D. A. (1987). *The Biomechanics and Motor Control of Human Movement*. University of Waterloo Press, 2 edition.